

The X-ray, Optical and Infrared Counterpart to GRB 980703

P.M. Vreeswijk¹, T.J. Galama¹, A. Owens², T. Oosterbroek², T.R. Geballe³, J. van Paradijs^{1,4}, P.J. Groot¹, C. Kouveliotou^{5,6}, T. Koshut^{5,6}, N. Tanvir⁷, R.A.M.J. Wijers⁸, E. Pian⁹, E. Palazzi⁹, F. Frontera^{9,10}, N. Masetti⁹, C. Robinson^{4,6}, M. Briggs^{4,6}, J.J.M. in 't Zand¹¹, J. Heise¹¹, L. Piro¹², E. Costa¹², M. Feroci¹², L.A. Antonelli¹², K. Hurley¹³, J. Greiner¹⁴, D.A. Smith¹⁵, A.M. Levine¹⁵, Y. Lipkin¹⁶, E. Leibowitz¹⁶, C. Lidman¹⁷, A. Pizzella¹⁷, H. Bönhardt¹⁷, V. Doublier¹⁷, S. Chaty^{18,19}, I. Smail²⁰, A. Blain²¹, J.H. Hough²², S. Young²³, N. Suntzeff²⁴

¹Astronomical Institute ‘Anton Pannekoek’, University of Amsterdam, & Center for High Energy Astrophysics, Kruislaan 403, 1098 SJ Amsterdam, The Netherlands

²Astrophysics Division, Space Science Department of ESA, European Space Research and Technology Centre, 2200 AG Noordwijk, The Netherlands

³Joint Astronomy Centre, 660 N. A’ohoku Place, Hilo, Hawaii 96720, USA

⁴Physics Department, University of Alabama in Huntsville, Huntsville AL 35899, USA

⁵Universities Space Research Association

⁶NASA/MSFC, Code ES-84, Huntsville AL 35812, USA

⁷Institute of Astronomy, Madingley Road, Cambridge CB3 0HA, UK

⁸Astronomy Program, State University of NY, Stony Brook, NY 11794-3800, USA

⁹Istituto Tecnologie e Studio Radiazioni Extraterrestri (TESRE), CNR, Via P. Gobetti 101, 40 129 Bologna, Italy

¹⁰Dipartimento di Fisica Universita’ di Ferrara, Via Paradiso 12, 44100 Ferrara, Italy

¹¹Space Research Organisation Netherlands (SRON), Sorbonnelaan 2, 3584 CA Utrecht, The Netherlands

¹²Istituto di Astrofisica Spaziale, CNR, Via Fosso del Cavaliere, Roma, I-00133, Italy

¹³University of California at Berkeley, Space Sciences Laboratory, Berkeley, CA, USA 94720-7450

¹⁴Astrophysikalisches Institut Potsdam, D-14482 Potsdam, Germany

¹⁵Massachusetts Institute of Technology, 77 Mass. Avenue, Cambridge, MA 02139-4307, USA

¹⁶Wise Observatory, Tel Aviv University, Ramat Aviv, Tel Aviv 69978, Israel

¹⁷ESO, Casilla 19001, Santiago 19, Chile

¹⁸DAPNIA/Service d’Astrophysique, CEA/Saclay, F-91191 Gif-Sur-Yvette, France

¹⁹Centre d’Etude Spatiale des Rayonnements, 9, avenue du Colonel Roche BP 4346, F-31

Received _____; accepted _____

028 Toulouse Cedex 4, France

²⁰University of Durham, South Road, Durham, DH1 3LE, UK

²¹Cavendish Laboratory, Madingley Road, Cambridge CB3 0HE, UK

²²Physics & Astronomy, University of Hertfordshire, Hatfield, AL10 9AB, UK

²³Cerro Tololo Interamerican Observatory, Casilla 603, La Serena, Chile

ABSTRACT

We report on X-ray, optical and infrared follow-up observations of GRB 980703. We detect a previously unknown X-ray source in the GRB error box; assuming a power law decline we find for its decay index $\alpha < -0.91$ (3σ). We invoke host galaxy extinction to match the observed spectral slope with the slope expected from ‘fireball’ models. We find no evidence for a spectral break in the infrared to X-ray spectral range on 1998 July 4.4, and determine a lower limit of the cooling break frequency: $\nu_c > 1.3 \times 10^{17}$ Hz. For this epoch we obtain an extinction of $A_V = 1.50 \pm 0.11$. From the X-ray data we estimate the optical extinction to be $A_V = 20.2_{-7.3}^{+12.3}$, inconsistent with the former value. Our optical spectra confirm the redshift of $z=0.966$ found by Djorgovski et al. (1998). We compare the afterglow of GRB 980703 with that of GRB 970508 and find that the fraction of the energy in the magnetic field, $\epsilon_B < 6 \times 10^{-5}$, is much lower in the case of GRB 980703, which is a consequence of the high frequency of the cooling break.

Subject headings: Gamma-rays bursts—gamma-rays:observations—radiation mechanisms:non-thermal

1. Introduction

Several properties of gamma-ray burst (GRB) afterglows can be well explained by ‘fireball’ models, in which a relativistically expanding shock front, caused by an energetic explosion in a central compact region, sweeps up the surrounding medium and accelerates electrons in a strong synchrotron emitting shock (Mészáros and Rees 1994, Wijers, Rees and Mészáros 1997; Sari, Piran and Narayan 1998; Galama et al. 1998a). The emission shows a gradual softening with time, corresponding to a decrease of the Lorentz factor of the outflow. Most X-ray and optical/infrared (IR) afterglows display a power law decay (except GRB 980425, which is most likely associated with the peculiar supernova SN 1998bw; Galama et al. 1998b).

Spectral transitions in the optical/IR have been detected for the afterglows of GRB 970508 (Galama et al. 1998a; Wijers and Galama 1998) and GRB 971214 (Ramaprakash et al. 1998). These have been explained by the passage through the optical/IR waveband of the cooling break, at ν_c (for GRB 970508) and the peak of the spectrum, at ν_m (for GRB 971214); see Sari, Piran & Narayan (1998) and Wijers & Galama (1998) for their definition. For GRB 970508 the observed break is in excellent agreement with such ‘fireball’ models, while for GRB 971214 an exponential extinction has been invoked to explain the discrepancy between the expected and observed spectral index.

GRB 980703 was detected on July 3.182 UT with the All Sky Monitor (ASM) on the *Rossi X-ray Timing Explorer* (RXTE; Levine et al. 1998), the *Burst And Transient Source Experiment* (BATSE, trigger No. 6891; Kippen et al. 1998), *BeppoSAX* (Amati et al. 1998) and *Ulysses* (Hurley et al. 1998). The burst as seen by BATSE consisted of two pulses, each lasting approximately 100 sec., with a total duration of about 400 sec. (Kippen et al. 1998). The first pulse had significant sub-structure, whereas the second, weaker episode was relatively smooth. This double-peak morphology has also been seen with the *BeppoSAX*

Gamma Ray Burst Monitor (Amati et al. 1998). BATSE measured a peak flux of $(1.9 \pm 0.1) \times 10^{-6}$ erg cm $^{-2}$ s $^{-1}$ (25 - 1000 keV) and fluence of $(4.6 \pm 0.4) \times 10^{-5}$ erg cm $^{-2}$ (> 20 keV), consistent with the *BeppoSAX* GRBM measurement. A time resolved spectral analysis of the burst will be presented elsewhere (Koshut et al. 1999).

Observations with the Narrow-Field Instruments (NFIs) of *BeppoSAX* showed a previously unknown X-ray source (Galama et al. 1998c) inside both the ASM error box and the InterPlanetary Network annulus (Hurley et al. 1998). Frail et al. (1998a; see also Zapatero Osorio et al. 1998) subsequently reported the discovery of a radio (6 cm) and optical (R-band) counterpart to GRB 980703.

Here we report X-ray (0.1-10 keV), optical (VRI), and infrared (JHK) follow-up observations of GRB 980703. In §2 we report our NFI X-ray observations of the ASM error box, and §3 is devoted to the description and results of our spectroscopic and photometric optical/IR monitoring campaign. We discuss the results of these observations in §4.

2. X-ray observations

We observed the ASM error box of GRB 980703 with the *BeppoSAX* Low- and Medium Energy Concentrator Spectrometers (LECS, 0.1-10 keV, Parmar et al. 1997; MECS, 2-10 keV, Boella et al. 1997) on July 4.10-5.08 UT (starting 22 hrs after the burst) and on July 7.78-8.71 UT. The LECS and MECS data show a previously unknown X-ray source 1SAX J2359.1+0835 at R.A. = 23^h59^m06^s.8, Decl. = +08°35'45" (equinox J2000.0), with an error radius of 50". The field also contains the sources 1SAX J2359.9+0834 at R.A. = 23^h59^m59^s, Decl.= +08°34'03", and 1SAX J0000.1+0817 at R.A. = 00^h00^m04^s, Decl.=+08°17'14". Both are outside the ASM error box, do not show any variability and coincide with the known ROSAT sources, 1RXS J235959.1+083355 and 1RXS

J000007.0+081653, respectively.

We extracted 1SAX J2359.1+0835 data at the best fit centroids with radii of 8' (LECS) and 2' (MECS). To analyze the spectrum we binned the data into channels, such that each contained at least 20 counts. Using the separate standard background files of the spectrometers, we simultaneously fitted the LECS and MECS data of July 4-5 UT, with a power law spectrum and a host galaxy absorption cut-off, using a redshift of $z = 0.966$ (Djorgovski et al. 1998; see also §3 of this paper). In the fit we fixed the Galactic foreground absorption at $N_{\text{H}} = 3.4 \times 10^{20} \text{ cm}^{-2}$ ($A_V = 0.19$, as inferred from the dust maps of Schlegel, Finkbeiner & Davis 1998¹, and the A_V - N_{H} relation of Predehl & Schmitt 1995). The average spectrum can be modelled with a photon index $\Gamma = 2.51 \pm 0.32$ and a host galaxy column density $N_{\text{H}}(\text{host}) = 3.6_{-1.3}^{+2.2} \times 10^{22} \text{ cm}^{-2}$, corresponding to $A_V(\text{host}) = 20.2_{-7.3}^{+12.3}$ (local to the absorber). Modelling the spectrum without $N_{\text{H}}(\text{host})$ results in a very poor fit. We did not account for a possible small position dependent error in the relative flux normalizations between the LECS and MECS, which is only a few percent near the center of the image. A change of 25% in the assumed Galactic foreground absorption does not affect the output values of the fit parameters. For the second epoch of NFI observations we kept the position fixed at the position determined from the first epoch; we find $F_X < 1.1 \times 10^{-13} \text{ erg cm}^{-2} \text{ s}^{-1}$ (3σ). Fitting a power law model to the light curve including the upper limit, we obtain $\alpha < -0.91$ for the decay index. The X-ray light curve is shown in Fig 1. We checked for the presence of the 6.4 keV K line at the redshifted energy of 3.26 keV, but do not detect it. The upper limit on its flux is $8.3 \times 10^{-6} \text{ photons cm}^{-2} \text{ s}^{-1}$ (90% confidence level), corresponding to an equivalent width of 532 eV in the observer's frame.

¹see <http://astro.berkeley.edu/davis/dust/index.html>

3. Optical and infrared observations

We observed the field of GRB 980703 with the Wise Observatory 1-m telescope (in I); the 3.5-m New Technology Telescope (NTT; in V, I and H), the 2.2-m (in H and Ks) and Dutch 90-cm (in gunn i) telescopes of ESO (La Silla); the CTIO 0.9-m telescope (in R) and UKIRT (in H, J and K).

The optical images were bias-subtracted and flat-fielded in the standard fashion. The infrared frames were reduced by first removing bad pixels and combining about five frames around each object image to obtain a sky image. This sky image was then subtracted after scaling it to the object image level; the resulting image was flat-fielded. Four reference stars were used to obtain the differential magnitude of the optical transient (OT) in each frame. These stars were calibrated by observing the standard stars PG2331+055 (in V and I; Landolt 1992), FS2 and FS32 (in J, H and K; Casali & Hawarden 1992). We used the R-band calibration of Rhoads et al. (1998). The offsets in right ascension and declination from the OT, and the apparent standard magnitudes outside the Earth’s atmosphere of the reference stars are listed in Table 1.

The light curves of the OT are shown in Fig. 2 (see Table 2 for a list of the magnitudes). In view of the flattening of the light curves after $t \sim 5$ days we fitted a model $F_\nu = F_0 \cdot t^\alpha + F_{\text{gal}}$ to our own I and H band light curves (in these bands we have sufficient data for a free parameter fit). Here t is the time since the burst in days, and F_{gal} is the flux of the underlying host galaxy. The values for $m_0 = -2.5 \cdot \log(F_0) + C$, the decay index α and $m_{\text{gal}} = -2.5 \cdot \log(F_{\text{gal}}) + C$, are listed in Table 3. The photometric calibration, which determines C , has been taken from Bessell (1979) for V, R and I and Bessell & Brett (1988) for J, H and K. The weighted mean value of α for the I and H-bands equals -1.61 ± 0.12 , while an I and H-band joint fit, with a single power law decay index, gives $\alpha = -1.63 \pm 0.12$ ($\chi = 15.4/16$). For the V, R, J and K bands we fixed α at -1.61 , included also data from the

literature, and fitted m_0 and m_{gal} . The fits are shown as solid lines in Fig. 2. We note that when we fit all three parameters to the R band data (mainly data from the literature) we obtain a temporal slope of -1.94 ± 0.22 , consistent with the adopted value of -1.61 ± 0.12 . However, we do not include this value in the average, since the R band magnitudes are taken from the literature and thus not consistently measured.

For four epochs we have reconstructed the spectral flux distribution of the OT (times t_1 , t_2 , t_3 and t_4 in Fig. 2, corresponding to 1998 July 4.4, 6.4, 7.6 and 8.4 respectively). The host galaxy flux, obtained from the fits to the light curves, was subtracted. We corrected the OT fluxes for Galactic foreground absorption ($A_V = 0.19$). If more than one value per filter was available around the central time of the epoch, we took their weighted average. All values were brought to the same epoch by applying a correction using the slope of the fitted light curve. For the first epoch (t_1) we fitted the resulting spectral flux distribution with a power law, $F_\nu \propto \nu^\beta$, and find $\beta = -2.71 \pm 0.12$.

We took three 1800 sec. spectra of the OT with the NTT, around July 8.38 UT. The #3 grism that was used has a blaze wavelength of 4600 Å and a dispersion of 2.3 Å/pixel. The slit width was set at 1". The three spectra were bias-subtracted and flat-fielded in the usual way. The co-added spectrum was then extracted the same way as the standard star Feige 110. We wavelength calibrated the spectrum with a Helium/Argon lamp spectrum, with a residual error of 0.03 Å. The spectrum was flux calibrated with the standard star Feige 110 (Massey et al. 1988). We estimate the accuracy of the flux calibration to be 10%. The wavelength and flux calibrated spectrum shows one clear emission line at 7330.43 ± 0.14 Å with a flux of $3.6 \pm 0.4 \times 10^{-16}$ erg cm⁻² s⁻¹. At the redshift $z = 0.966$ determined by Djorgovski et al. (1998) this is the $\lambda 3727$ line of [O II]; our wavelength measurement corresponds to $z = 0.9665 \pm 0.0005$.

4. Discussion

From the optical/IR light curves presented in §3 we have obtained an average power law decay constant $\alpha = -1.61 \pm 0.12$. This value is consistent with the ones derived by Bloom et al. (1998) ($\alpha_R = -1.22 \pm 0.35$, and $\alpha_I = -1.12 \pm 0.35$) and Castro-Tirado et al. (1999) ($\alpha_R = -1.39 \pm 0.3$, and $\alpha_H = -1.43 \pm 0.11$).

If we make the assumption that the OT emission is due to synchrotron radiation from electrons with a power law energy distribution (with index p), one expects a relation between p , the spectral slope β , and the decay constant α (Sari, Piran and Narayan 1998). We assume that our observations are situated in the slow cooling, low frequency regime (e.g. for GRB 970508 this was already the case after 500 sec.; Galama et al. 1998a). One must distinguish two cases: (i) both the peak frequency ν_m and the cooling frequency ν_c are below the optical/IR waveband. Then $p = (-4\alpha + 2)/3 = 2.81 \pm 0.16$ and $\beta = -p/2 = -1.41 \pm 0.08$, (ii) ν_m has passed the optical/IR waveband, but ν_c has not yet. In that case $p = (-4\alpha + 3)/3 = 3.15 \pm 0.16$ and $\beta = -(p - 1)/2 = -1.07 \pm 0.08$. In both cases the expected value of β is inconsistent with the observed $\beta = -2.71 \pm 0.12$. Following Ramaprakash et al. (1998) we assume that the discrepancy is caused by host galaxy extinction (note that we have already corrected the OT fluxes for Galactic foreground absorption). To determine the host galaxy absorption we first blueshifted the OT flux distribution to the host galaxy rest frame (using $z = 0.966$), and then applied an extinction correction using the Galactic extinction curve of Cardelli, Clayton & Mathis (1989), to obtain the expected spectral slope β . For epoch t_1 (July 4.4 UT), we obtain $A_V = 1.15 \pm 0.13$ and $A_V = 1.45 \pm 0.13$ for the cases (i) and (ii), respectively (see Fig. 3).

In case (i) we find that an extrapolation of the optical flux distribution to higher frequencies predicts an X-ray flux that is significantly below the observed value, whereas in case (ii) the extrapolated and observed values are in excellent agreement. The mismatch in

case (i) is in a direction that cannot be interpreted in terms of the presence of a cooling break between the optical and X-ray wavebands. When we include the X-ray data point in the fit to obtain a more accurate determination of A_V , we find $A_V = 1.50 \pm 0.11$, and $\beta = -1.013 \pm 0.016$. We conclude that the optical/IR range is not yet in the cooling regime, and so $p = 3.15 \pm 0.16$. Where would the cooling frequency, ν_c , be located? The X-ray photon index, $\Gamma = 2.51 \pm 0.32$, corresponding to a spectral slope of $\beta = -1.51 \pm 0.32$ suggests that perhaps the X-ray waveband is just in the cooling regime, in which case the expected local X-ray slope would be $\beta = -p/2 = -1.57 \pm 0.08$, while if not in the cooling regime, it would be $\beta = -(p - 1)/2 = -1.07 \pm 0.08$. However, the large error on the measured X-ray spectral slope would also allow the cooling break to be above 2-10 keV. We estimate the (2σ) lower limit to the cooling frequency to be $\nu_c > 1.3 \times 10^{17}$ Hz ($h\nu_c > 0.5$ keV).

We performed the same analysis for the other epoch (t_4) with X-ray data (see Fig. 3). At this epoch, the X-ray upper limit does not allow us to discriminate between the two cases. However, we can still estimate a lower limit to the cooling break from its time dependence: $\nu_c \propto t^{-1/2}$, which would allow the break to drop to $\nu_c > 6.3 \times 10^{16}$ Hz only, between epoch t_1 and t_4 .

On the basis of our analysis we conclude that there is no strong evidence for a cooling break between the optical/IR and the 2-10 keV passband before 1998 July 8.4 UT. This conclusion is at variance with the inference of Bloom et al. (1998), who infer from their fits that there is a cooling break at about 10^{17} Hz. Upon closer inspection, there is no real disagreement: Bloom et al. found a slightly shallower temporal decay, and therefore a bluer spectrum of the afterglow, which causes their extrapolated optical spectrum to fall above the X-ray point. However, their error of 0.35 on the temporal decay leads to an error of 0.24 on their predicted spectral slope, and this means that a 1σ steeper slope in their Fig.

2 would be consistent with no detected cooling break.

Assuming that the spectral slope ($\beta = -1.013 \pm 0.016$) did not change during the time spanned by the four epochs $t_1 - t_4$ (as suggested by the lack of evidence for a break in the light curve during this timespan) we have derived the V-band extinction A_V as a function of time: $A_V = 1.50 \pm 0.11, 1.38 \pm 0.35, 0.84 \pm 0.29$ and 0.90 ± 0.25 for the epochs 1 through 4, respectively. Fitting a straight line through these, we obtain a slope of -0.16 ± 0.06 , i.e. not consistent with zero at the 98.8% confidence level. Such a decrease of the optical extinction, A_V , might be caused by ionization of the surrounding medium (Perna and Loeb 1997).

The V-band extinction $A_V = 20.2_{-7.3}^{+12.3}$, derived from the host galaxy N_H fit to the MECS and LECS data (July 4-5 UT) is not in agreement with $A_V = 1.50 \pm 0.11$ as derived from the fit from the optical spectral flux distribution. This may be due to a different dust to gas ratio for the host galaxy of GRB 980703, or a higher abundance than normal of the elements that cause the X-ray absorption.

With the above derived constraint on ν_c we can partially reconstruct the broad-band flux distribution of the afterglow of GRB 980703: from the radio observations of Frail et al. (1998b) at 1.4, 4.86 and 8.46 GHz, we determine the self-absorption frequency ν_a and its flux F_{ν_a} from the fit $F_\nu = F_{\nu_a}(\nu/\nu_a)^2(1 - \exp[-(\nu/\nu_a)^{-5/3}])$ to the low-energy part of the spectrum (e.g. Granot, Piran and Sari 1998). We have used averages of the 1.4 and 4.86 GHz observations to obtain best estimates of the radio flux densities as particularly those frequencies suffer from large fluctuations due to interstellar scintillation (Frail et al. 1998b). We find $\nu_a = 3.68 \pm 0.33$ GHz and $F_{\nu_a} = 789 \pm 42$ μ Jy. (The fit is shown in Fig. 4.) The intersection of the extrapolation from the low-frequency to the high-frequency fit gives a rough estimate of the peak frequency, $\nu_m \sim 4 \times 10^{12}$ Hz, and of the peak flux, $F_{\nu_m} \sim 8$ mJy (see Fig. 4). By assuming such a simple broken power law spectrum the peak flux density

will likely be overestimated (realistic spectra are rounder at the peak); it is clear from Fig. 4 that $1 < F_{\nu_m} < 8$ mJy.

Following the analysis of Wijers and Galama (1998) we have determined the following intrinsic fireball properties: (i) the energy of the blast wave per unit solid angle: $\mathcal{E} > 5 \times 10^{52}$ erg/(4π sterad), (ii) the ambient density: $n > 1.1$ nucleons cm^{-3} , (iii) the percentage of the nucleon energy density in electrons: $\epsilon_e > 0.13$, and (iv) in the magnetic field: $\epsilon_B < 6 \times 10^{-5}$. The very low energy in the magnetic field, ϵ_B , is a natural reflection of the high frequency of the cooling break ν_c .

We have compared this afterglow spectrum with that of GRB 970508. Scaling the latter in time according to $\nu_a \propto t^0$, $\nu_m \propto t^{-3/2}$ and $\nu_c \propto t^{-1/2}$, the results of GRB 970508 (Galama et al. 1998a; see also Granot, Piran and Sari 1998) would correspond to $\nu_a \sim 2.3$ GHz, $\nu_m = 2.8 \times 10^{12}$ Hz, $\nu_c = 4.8 \times 10^{14}$ Hz, and $F_{\nu_m} = 1.3$ mJy. In this calculation we have corrected for the effect of redshift (see Wijers and Galama 1998) such that the values represent GRB 970508, were it at the redshift of GRB 980703 and observed 1.2 days after the event. The greatest difference between the two bursts is in the location of the cooling frequency, ν_c .

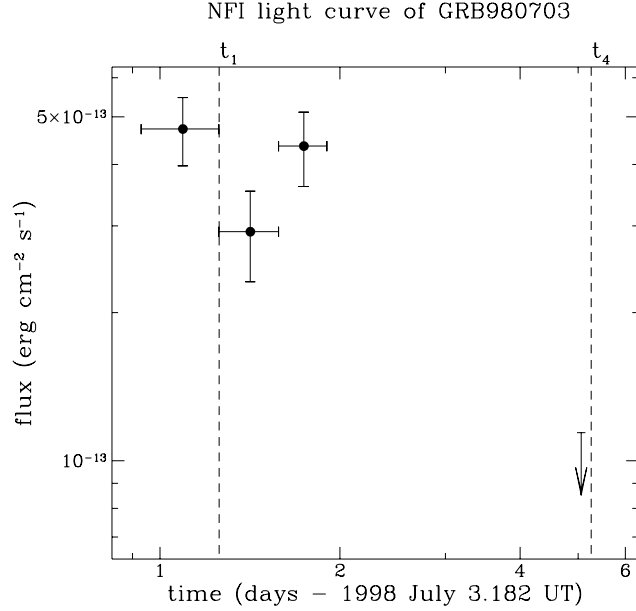
The observations on the United Kingdom Infrared Telescope, which is operated by the Joint Astronomy Centre on behalf of the U.K. Particle Physics and Astronomy Research Council, were carried out in Service mode by UKIRT staff. The BeppoSAX satellite is a joint Italian and Dutch programme. PMV is supported by the NWO Spinoza grant. TJG is supported through a grant from NFRA under contract 781.76.011. CK acknowledges support from NASA grant NAG 5-2560. TO acknowledges an ESA Fellowship. KH is grateful for support under JPL Contract 958056 for Ulysses, and under NASA grant NAG 5-1560 for IPN operations.

REFERENCES

- Amati, L., et al. 1998, GCN circular, 146
- Bessell, M.S. 1979, PASP, 91, 589
- Bessell, M.S. & Brett, J.M. 1988, PASP, 100, 1134
- Bloom, J.S., et al. 1998, ApJ, 508, L21
- Boella, G., et al. 1997, A&AS, 122, 299
- Cardelli, J.A., Clayton, G.C. & Mathis, J.S. 1989, ApJ, 345, 245
- Castro-Tirado, A.J. et al. 1999, ApJ, 511, L85
- Casali, M.M. & Hawarden, T.G. 1992, JCMT-UKIRT Newsletter, No. 3, 33
- Djorgovski, S.G., et al. 1998, ApJ, 508, L17
- Frail, D.A., et al. 1998a, GCN circular, 128
- Frail, D.A., et al. 1998b, GCN circular, 141
- Galama, T.J., et al., 1998a, ApJ, 500, L97
- Galama, T.J., et al. 1998b, Nature, 395, 670
- Galama, T.J., et al. 1998c, GCN circular, 127
- Granot, J., Sari, T. and Sari, R. 1998, submitted, astro-ph/9808007
- Henden, A.A., et al. 1998, GCN circular, 131
- Hurley, K., et al. 1998, GCN circular, 125
- Kippen, M., et al. 1998, GCN circular, 143
- Koshut, T., et al. 1999, in preparation
- Landolt, A.U. 1992, AJ 104, 340
- Levine, A., et al. 1998, IAU Circ., 6966
- Massey, P., et al. 1988, ApJ, 328, 315
- Mészáros, P. & Rees, M.J. 1994, MNRAS, 269, L41
- Parmar, A.N., et al. 1997, A&AS, 122, 309
- Pedersen, H., et al. 1998, GCN circular, 142

- Perna, R. & Loeb, A. 1998, ApJ, 501, 467
- Predehl, P. and Schmitt, J.H.M.M. 1995, A&A, 293, 889
- Ramaprakash, A.N., et al. 1998, Nature, 393, 43
- Rhoads, J., et al. 1998, GCN circular, 144
- Sari, R., Piran, T., Narayan, R. 1998, ApJ, 497, L17
- Schlegel, D.J., Finkbeiner, D.P. and Davis, M. 1998, ApJ, 500, 525
- Sokolov, V., et al. 1998, GCN circular, 147
- Wijers, R.A.M.J. and Galama, T.J. 1998, in press, ApJ
- Wijers, R.A.M.J., Rees, M.J. and Mészáros, P. 1997, MNRAS, 288, L51
- Zapatero Osorio, M.R., et al. 1998, IAU Circ., 6967

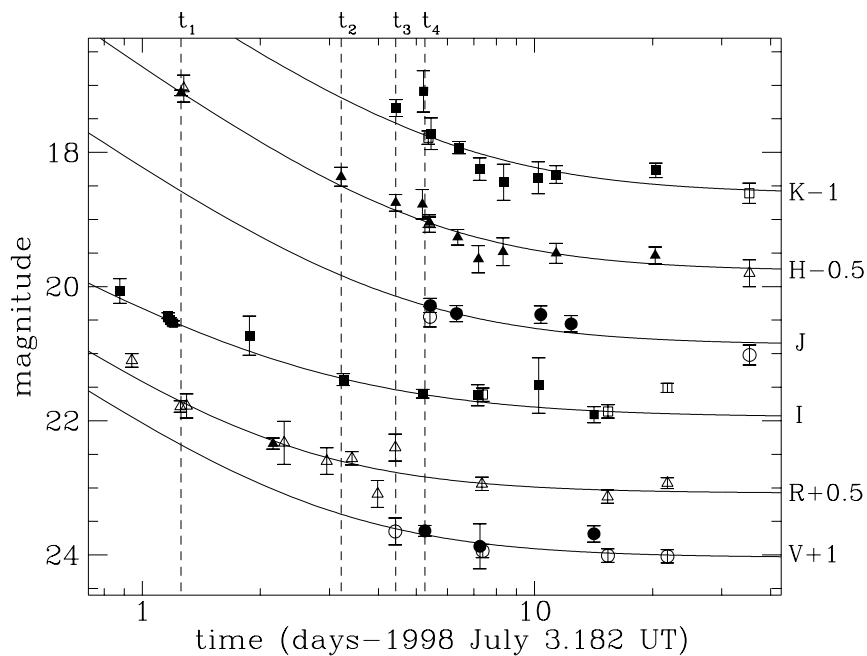
Fig. 1.— The 2-10 keV light curve of GRB 980703. Time and flux are on a logarithmic scale.



filter	star 1	star 2	star 3	star 4
Δ R.A.($''$)	-18.0	-11.7	-8.0	-13.9
Δ Decl.($''$)	3.9	-9.7	-21.7	-31.8
V	21.33 \pm 0.06	17.02 \pm 0.05	22.06 \pm 0.08	22.68 \pm 0.12
R	20.39 \pm 0.04	16.64 \pm 0.02	20.72 \pm 0.05	
I	19.55 \pm 0.07	16.30 \pm 0.05	19.21 \pm 0.06	20.01 \pm 0.08
J	18.45 \pm 0.13	15.75 \pm 0.11	17.52 \pm 0.12	18.25 \pm 0.13
H	17.85 \pm 0.12	15.44 \pm 0.10	16.96 \pm 0.11	17.69 \pm 0.12
K	17.71 \pm 0.13	15.41 \pm 0.12	16.72 \pm 0.12	17.52 \pm 0.13

Table 1: The magnitudes and offset from the OT in arc seconds of the four comparison stars used. The error is the quadratic average of the measurement error (Poisson noise) and a constant offset, which we estimate to be 0.05 for the optical passbands and 0.1 for the infrared filters.

Fig. 2.— V, R, I, J, H and K light curves of GRB980703. The filled symbols denote our data, while the open symbols represent data taken from the literature (Zapatero Osorio et al. 1998; Rhoads et al. 1998; Henden et al. 1998; Bloom et al. 1998; Pedersen et al. 1998; Djorgovski et al. 1998; Sokolov et al. 1998 & private communication). For each filter a power law model plus a constant: $F_\nu = F_0 \cdot t^\alpha + F_{\text{gal}}$ is fitted (solid lines). The fit parameters are listed in Table 3. The times $t_1 - t_4$, at which we have reconstructed the spectral flux distribution of the OT, are indicated by the dashed lines.



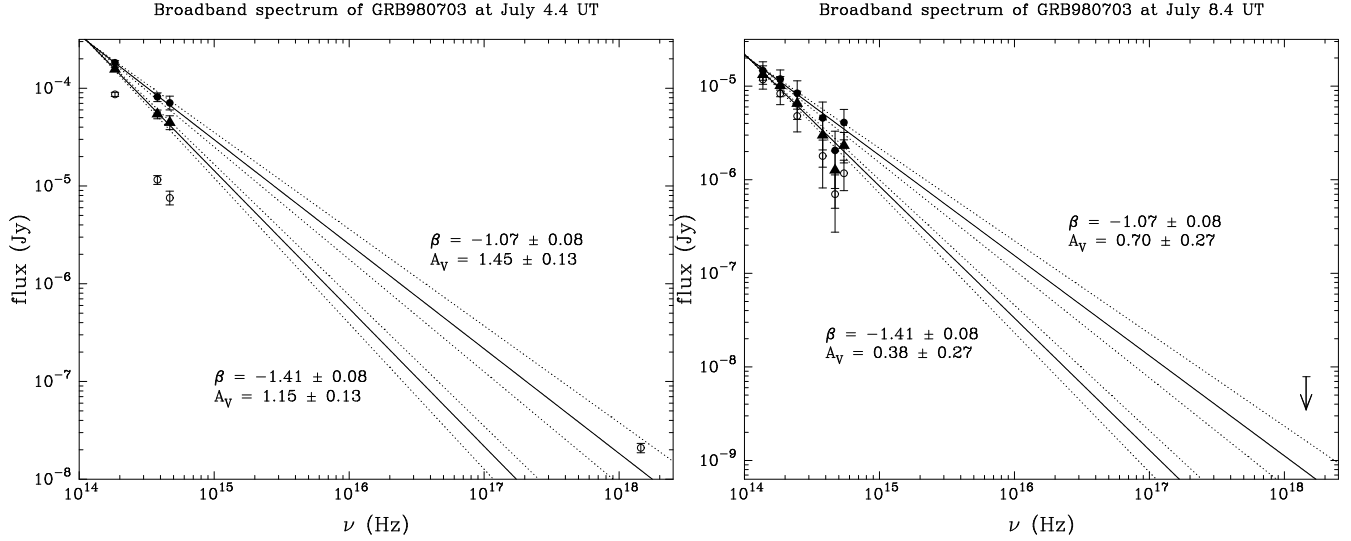


Fig. 3.— Left figure: Broad-band spectrum of GRB980703 at July 4.4 UT (i.e., at t_1 in Fig. 2). The open symbols are the R, I and H OT fluxes (interpolated to July 4.4, corrected for Galactic foreground absorption and the host galaxy flux) and the MECS (2-10 keV) de-absorbed flux (the absorption correction is 7%). The filled symbols are obtained by invoking an interstellar extinction, A_V , to force the slope of the data points to take on the two possible theoretical spectral slopes. The two slopes β and their 1σ errors are indicated by the solid and dotted lines. Right figure: Broad-band spectrum of GRB980703 at July 8.4 UT (i.e., at t_4 in Fig. 2). The open symbols are the V, R, I, J, H and K OT fluxes and the MECS (2-10 keV) de-absorbed 3σ upper limit.

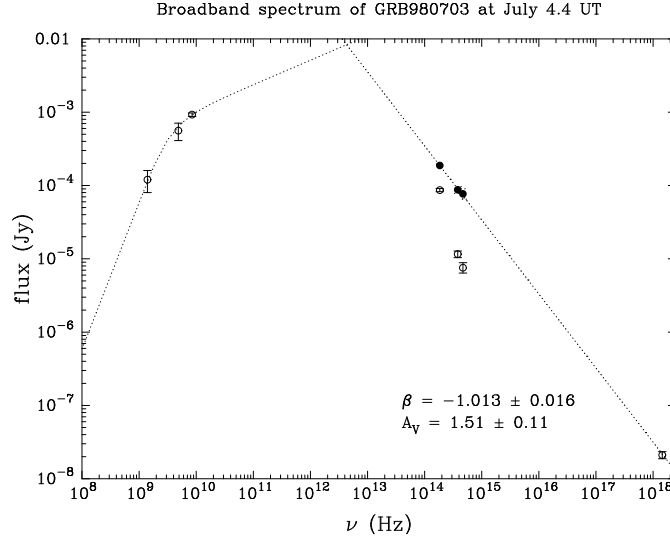


Fig. 4.— Radio to X-ray spectrum of GRB980703 at July 4.4 UT (i.e., at t_1 in Fig. 2). Shown are data from Fig. (3) as well as 1.4, 4.86 and 8.46 GHz observations from Frail et al. (1998b). The fit $F_\nu = F_{\nu_a}(\nu/\nu_a)^2(1 - \exp[-(\nu/\nu_a)^{-5/3}])$ to the low-energy part of the spectrum with $\nu_a = 3.68 \pm 0.33$ GHz and $F_{\nu_a} = 789 \pm 42$ μ Jy is shown by the dotted line. The best fit to the optical/IR and X-ray data is also shown.

UT date (1998 July)	magnitude	filter	exp. time (seconds)	seeing (")	telescope/reference
4.059	20.07 ± 0.19	I	2100	2.39	Wise 1-m
4.347	20.43 ± 0.04	I	900	1.16	ESO NTT (EMMI)
4.359	20.49 ± 0.03	I	900	1.10	ESO NTT (EMMI)
4.372	20.54 ± 0.03	I	900	1.14	ESO NTT (EMMI)
4.383	20.55 ± 0.04	I	900	1.02	ESO NTT (EMMI)
4.439	17.61 ± 0.04	H	810		ESO NTT (SOFI)
5.059	20.73 ± 0.29	I	1800	3.09	Wise 1-m
5.339	21.84 ± 0.08	R	3600	1.86	CTIO 0.9-m
6.395	18.86 ± 0.14	H	540		ESO NTT (SOFI)
7.609	19.25 ± 0.12	H	1200		UKIRT
7.622	18.36 ± 0.13	K	600		UKIRT
8.361	19.27 ± 0.22	H	2700		ESO 2.2m
8.375	21.60 ± 0.06	I	900	0.92	ESO NTT (EMMI)
8.396	18.14 ± 0.35	Ks	2700		ESO 2.2m
8.438	22.64 ± 0.08	V	900	1.93	ESO NTT (EMMI)
8.578	19.54 ± 0.08	H	1620		UKIRT
8.608	20.28 ± 0.10	J	2160		UKIRT
8.633	18.77 ± 0.24	K	600		UKIRT
9.509	20.40 ± 0.12	J	2160		UKIRT
9.554	19.76 ± 0.12	H	2160		UKIRT
9.614	18.94 ± 0.09	K	2160		UKIRT
10.353	21.62 ± 0.16	gunn i	4800	1.22	ESO Dutch
10.380	20.09 ± 0.20	H	3750		ESO 2.2m
10.435	19.24 ± 0.16	Ks	3900		ESO 2.2m
10.440	22.87 ± 0.34	V	900	1.06	ESO NTT (EMMI)
11.496	19.98 ± 0.21	H	2160		UKIRT
11.527	19.47 ± 0.27	K	2160		UKIRT
13.414	18.76 ± 0.30	Ks	4950		ESO 2.2m
13.438	21.47 ± 0.41	gunn i	2400	1.98	ESO Dutch
13.558	20.42 ± 0.13	J	2160		UKIRT
14.536	20.00 ± 0.15	H	2160		UKIRT
14.545	19.36 ± 0.14	K	2160		UKIRT
15.582	20.56 ± 0.12	J	3240		UKIRT
17.359	22.68 ± 0.12	V	900	1.05	ESO NTT (SUSI2)
17.371	21.91 ± 0.12	I	900	0.75	ESO NTT (SUSI2)
23.501	20.04 ± 0.12	H	4860		UKIRT
23.578	19.28 ± 0.11	K	4860		UKIRT

Table 2: The log of the observations with the columns: UT Date, magnitude and error, filter, exposure time, seeing and the telescope. Instruments and CCDs used: NTT EMMI: red arm with TEK 2k × 2k CCD (#36), 0.27"/pixel; NTT SUSI2: EEV 4k × 2k CCD (#45 & #46), 0.08"/pixel; NTT SOFI: Hawaii 1k × 1k HgCdTe array, 0.29"/pixel; ESO Dutch: CCD Camera with TEK 512 × 512 CCD (#33), 0.47"/pixel; Wise 1-m: TEK 1k × 1k CCD, 0.70"/pixel; CTIO 0.9-m: TEK 2k × 2k CCD, 0.38"/pixel; UKIRT: IRCAM3 with FPA42 256 × 256 detector, 0.29"/pixel; 2.2-m (IRAC2b): NICMOS-3 256 × 256 array, 0.507"/pixel. We note that we do not list an estimate of the seeing in case of infrared observations, since the real seeing is overestimated due to the process of co-adding the individual frames.

Table 3: Fit parameters for the model $m = -2.5 \log(10^{-0.4 m_0} t^\alpha + 10^{-0.4 m_{gal}})$

filter	m_0	α	m_{gal}	χ_{red}^2
V	$21.22^{+0.48}_{-0.33}$	-1.61	$23.04^{+0.08}_{-0.08}$	5.5/5
R	$21.18^{+0.09}_{-0.08}$	-1.61	$22.58^{+0.06}_{-0.05}$	14.7/10
I	$20.60^{+0.04}_{-0.04}$	$-1.36^{+0.27}_{-0.36}$	$21.95^{+0.25}_{-0.16}$	4.5/8
J	$18.32^{+0.33}_{-0.25}$	-1.61	$20.87^{+0.07}_{-0.11}$	5.6/4
H	$17.29^{+0.06}_{-0.06}$	$-1.67^{+0.13}_{-0.15}$	$20.27^{+0.19}_{-0.15}$	6.5/7
K	$16.48^{+0.18}_{-0.15}$	-1.61	$19.62^{+0.12}_{-0.11}$	11.3/9